ACS APPLIED MATERIALS & INTERFACES

Research Article

www.acsami.org

Digital Controlled Luminescent Emission via Patterned Deposition of Lanthanide Coordination Compounds

Hua-Bin Zhang, Meng Liu, Xiaoping Lei, Tian Wen, and Jian Zhang*

State Key Laboratory of Structural Chemistry, Fujian Institute of Research on the Structure of Matter, Chinese Academy of Sciences, Fuzhou, Fujian 350002, China

Supporting Information

ABSTRACT: Presented here is a new direct patterning method, printer-type lithography technology, for the formation of lanthanide coordination compounds (LCCs) single crystal in different spatial locations. We first integrate this technology in digital controlled emission by patterned deposition of LCCs. We demonstrate its usefulness in the control of emission intensity by regulating print cycles, so that the emission intensity can be digitally controlled. This printer technology can also be used to precisely control the location at which a single LCC crystal is grown, which provides great promise in the application of anticounterfeiting barcode. Besides, by varying the stoichiometric ratio of the lanthanide ions in the identical cartridge, a fluent change of emission colors from white, orange, pink, to blue green was achieved. Therefore, this low-cost and high-throughput patterning technique can be readily applied to a wide range of areas including micro-/nanofabrication, optics, and electronics studies.

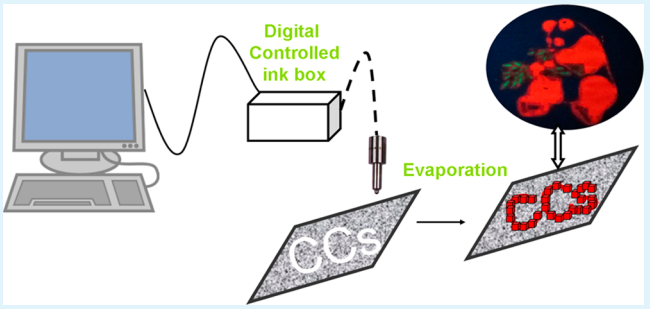

KEYWORDS: *controlled emission, patterned deposition, lanthanide coordination compounds, spatial location, luminescent emission*

INTRODUCTION

Lanthanide coordination compounds (LCCs) are of great importance, not only because of their fascinating architectures but also due to their potential applications in diagnostic tools, luminescence sensors, and light-emitting devices (LEDs).[1−7] For the application as smart membrane, lighting apparatus, or sensing device, the LCCs single crystals should be immobilized at specific locations on surface rather than being a free-flowing powder, and thus the spatially and morphologically controlled growth of LCCs films on various surfaces gained significant importance.[8−11] To realize the deposition of LCCs, a number of interesting methods have been developed, including in situ (hydrothermal) growth, dip-coating, layer-by-layer growth, electrochemical deposition, spray-coating, and evaporation/solvent-induced growth. Although these methods mostly yield uniform films, the precise positioning, crystallographic orientation, as well as quantitative control, which are crucial for integrated device fabrication, are far from reach.[10,12−14] Efficient patterning techniques, which integrate applications of microfluidic and electronic devices, present a technological breakthrough in this area. Nevertheless, most of the patterning techniques, such as soft lithography, photolithography, deep X-ray lithography, and electron-beam lithography, consist of complicated multistep procedures and are typically limited to relatively small overall areas.[15−19] Thus, the development of an effective and general method for the controlled deposition of LCCs and further realizing the digital controlled emission is much desirable.

The key issue to realizing the digital controlled emission for LCCs is to tune the chemical component and control the spatial distribution of single crystals.[20−22] One could imagine delivering droplets of a solution containing LCCs onto specific regions of a surface. Once these droplets were positioned on the surface, the formation and crystallization of LCCs could be confined within each deposited droplet by controlling its evaporation and/or using external conditions, such as microwave radiation or high temperature. Printer-type lithography, in which the droplet can be transferred and patterned directly onto the substrate from a nozzle or print head, seems an elegant platform to realize the deposition of LCC single crystals in desired spatial distribution. In fact, this technology has been successfully applied in the printing of organic compounds and semiconducting materials with the aim of achieving "printed electronics".[23−27] However, printer-type lithography has not been used for the patterned deposition of LCC single crystals.[28,29]

In this work, we wish to demonstrate that printer-type lithography, even with a commercial, off-the-shelf inkjet printer, is a straightforward route to deposit patterned LCC single crystals onto various flexible substrates. The evaporation-induced crystallization from a stable precursor solution containing the metals and the organic building blocks is considered as a effective approach to grow the crystals, and

Received: April 29, 2014
Accepted: July 8, 2014
Published: July 8, 2014

   dx.doi.org/10.1021/am502559v | ACS Appl. Mater. Interfaces 2014, 6, 12594−12599

such a precursor solution can serve as "ink".[10,30,31] Because of the crucial role of the viscosity and surface tension of the ink for the inkjet printing process, we introduce Olefin E1010 (acetylene glycol-based surfactant) in a certain ratio into the precursor solutions to reduce the surface tension. When this solution was used as ink, the desired patterns could be easily obtained by printing, followed by evaporation at room temperature. Here, we focus on the patterned deposition of a highly luminescent material $[H_2NMe_2]_3[Ln(dipic)_3]$ (**1**) (H_2dipic = pyridine-2,6-dicarboxylic acid) on different supports and attempt to build a platform for digital controlled luminescent emission.[32]

EXPERIMENTAL SECTION

Synthesis of Compound $[H_2NMe_2]_3[Ln(dipic)_3]$ (1). The synthesis of **1** has been previously reported by using DMF (*N*,*N*-dimethylformamide) as the solvent, and long reaction time was required.[33] The heavy use of DMF generates a large amount of byproduct, which is harmful to the environment. Here, we develop an environment-friendly synthesis route. The mixture of $Ln(NO_3)_3{\cdot}6H_2O$ (Ln = Eu, Gd, or Tb), 2,6-H_2dpa, and dimethylamine with 1:3:3 ratio in ultrapure water was stirred at room temperature for 1 h, resulting in the formation of a clear solution. Evaporation of this solution produced colorless crystals of compound **1** in high yield (>90%). PXRD studies further demonstrated the phase purity of **1** (Supporting Information Figure S1).

Preparation of the Precursor Solution for Ink. By dissolving 1 mmol of $Ln(NO_3)_3{\cdot}H_2O$, 3 mmol of H_2dipic, and 3 mmol of dimethylamine in 10 mL of ultrapure water, a clear solution was prepared. For the preparation of precursor solution, 5 mL of olefin E1010 (content of 1%) was added under vigorous stirring. Finally, the mixture was filtered through a 0.2 μm syringe filter. The obtained clear solution can be used as "ink" without further treatment. The mixed $Eu_xTb_yGd_{1-x-y}$ precursor solution was prepared by using a mixture of $Eu(NO_3)_3{\cdot}6H_2O$, $Tb(NO_3)_3{\cdot}6H_2O$, and $Gd(NO_3)_3{\cdot}6H_2O$ in a certain ratio as the metal source through the same procedure.

Pattern Deposition by the Precursor Solutions. **1**-Eu, **1**-Tb, and **1**-Gd "ink" precursors (13 mL) were loaded into empty cartridges (designated as "blank, yellow, and blue ink cartridge" by the Epson coding), respectively. The excess ink was wiped with paper before being loaded into printer head. After the desired patterns were printed, the substrate was evaporated under room temperature for 10 min. For the multiple "printing−drying" cycles, the dried substrate was loaded again by carefully adjusting it to the same position before printing.

RESULTS AND DISCUSSION

As shown in Figure 1, the ink can be transferred from digital controlled ink cartridges into nozzle and then printed onto special positions. Further, evaporation development steps caused the formation of monodispersed crystals of LCCs in desired pattern by in situ crystallization. As no crystallization is

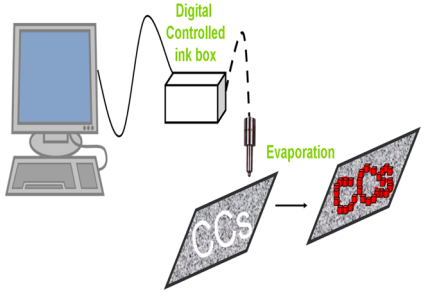

Figure 1. Schematic representation of the process for the printing of LCC crystals.

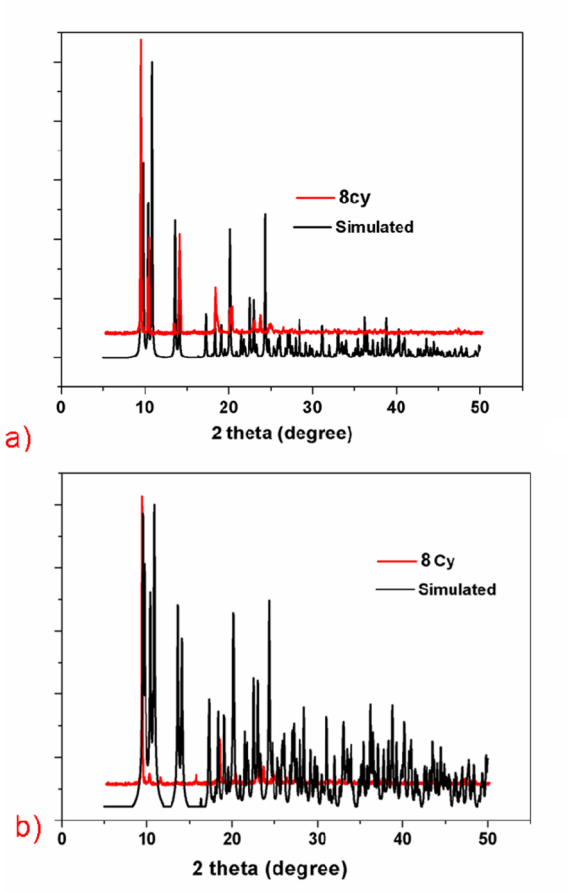

Figure 2. (a) Comparison between LCCs SXRD pattern in A4 paper and the simulated pattern from single-crystal X-ray data of **1**. (b) Comparison between LCCs SXRD pattern in plastic film and the simulated pattern from single-crystal X-ray data of **1**.

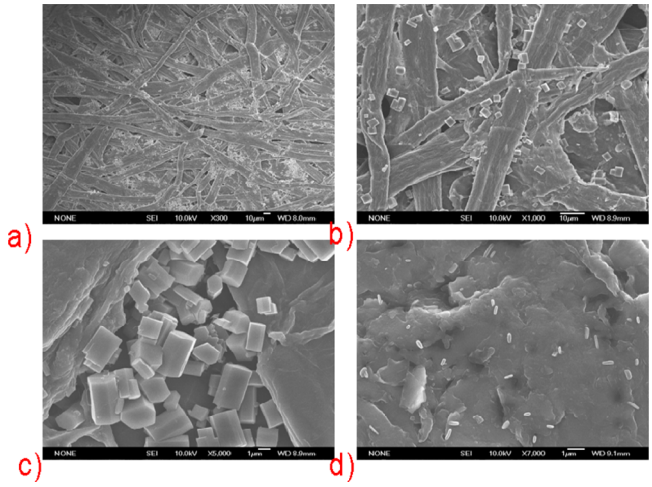

Figure 3. (a−c) SEM images of LCCs printed on paper under different resolution. (d) SEM images of LCCs printed on plastic film.

observed in precursor solution kept in a closed container at the same temperature, evaporation is the main driving force for nucleation. The surface deposition of the LCCs was well investigated by surface X-ray diffraction (SXRD) and scanning electron microscopy (SEM). The density and thickness of films could be simply controlled by printing the designed patterns for

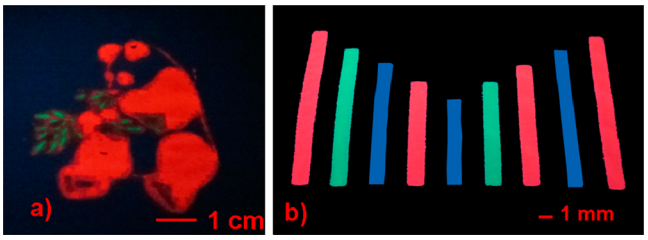

Figure 4. (a) To demonstrate the applicability for large area patterning, China's treasure-panda was printed by using LCCs inks. (b) Presentation of anticounterfeiting barcode (**1**-Eu, **1**-Gd, and **1**-Tb, utilized as red, blue, and green emission sources, respectively).

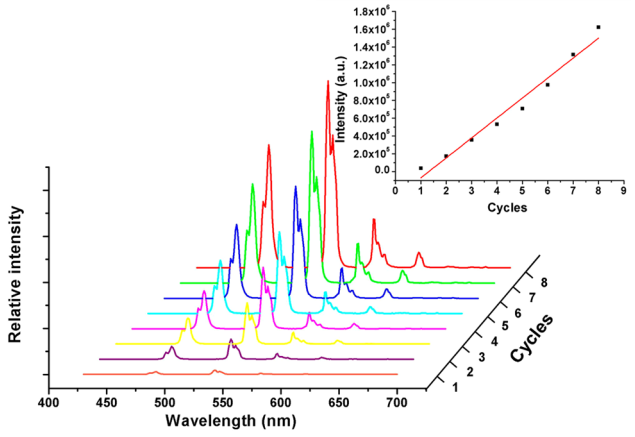

Figure 5. Line profiles of the emission spectra for different deposition cycles. Inset: Linear relationship between the emission intensity at 544 nm and print cycles.

Table 1. Molar Ratios of Multicomponent $Gd^{3+}/Eu^{3+}/Tb^{3+}$ for Samples with Varied Color Coordinates

		mole ratios of multicomponents		
approximate color regions	CIE (*x y*)	Gd	Eu	Tb
white	(0.34, 0.35)	0.920	0.048	0.032
pink	(0.35, 021)	0.990	0.007	0.003
yellow green	(0.31, 0.46)	0.80	0.05	0.15
orange	(0.56, 0.32)	0.97	0.02	0.01

multiple "printing−evaporation" cycles (abbreviated as ncy in the following). For this, 1cy to 8cy of LCCs was printed onto A4 paper. Visual inspection shows that the printed LCCs paper keeps its original appearance even after 8cy (Supporting Information Figure S3). The chemical identity of the LCCs films was confirmed by comparison of the SXRD pattern with the simulated X-ray reflection pattern (Figure 2a). Interestingly, SEM images (Figure 3a−c) indicate that the printed area was basically completely covered by monodispersed particles of compound **1**. The printed sample with well-shaped cubic crystals on A4 paper has edge dimensions between 2.3 and 4 μm, indicating a relative uniform size distribution of the printed crystals. As shown in Supporting Information Figure S4a, well-shaped crystals of compound **1** were grown in the contact areas of the paper, and the adherence of the crystallites to the paper underneath is quite strong as evidenced by the destructive experience. After crystals were broken by grinding, the samples still can adhere to the surface of the paper (Supporting Information Figure S4). This strong connection is attributed to the high roughness of the paper substrate. It is well-known that substrate surface properties play an important role in the interface growth. To provide further evidence of the formation

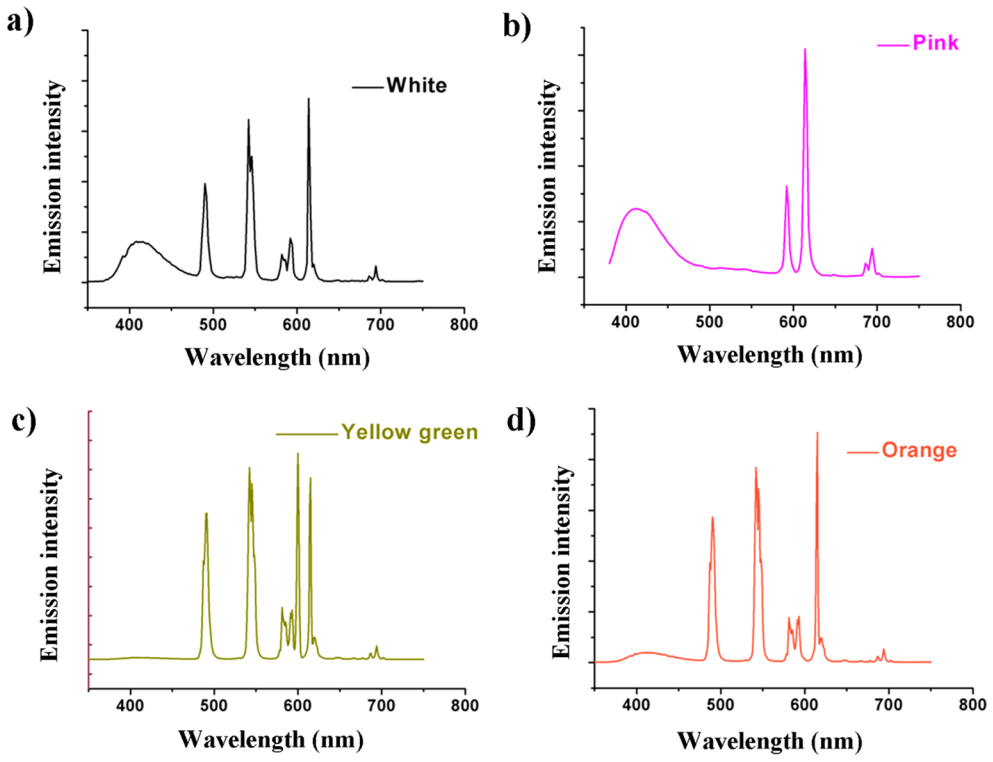

Figure 6. Emission spectra for printing mixed-lanthanide luminescence at room temperature under UV excitation at 295 nm: (a) white emission; (b) pink emission; (c) yellow green emission; and (d) orange emission.

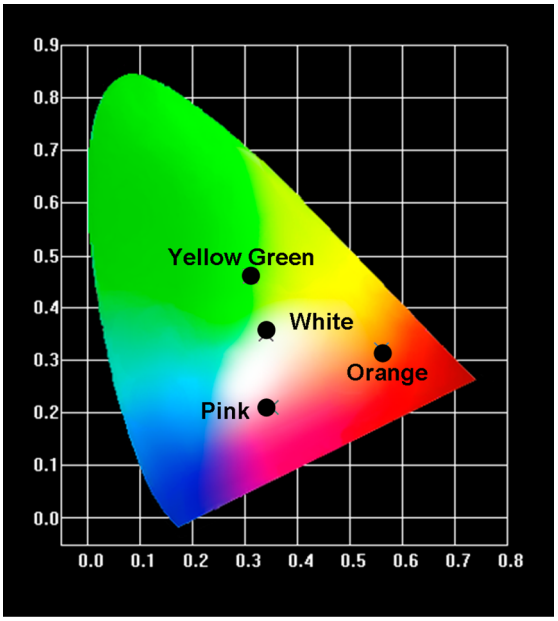

Figure 7. CIE chromaticity diagram showing the location of the multicolored photoluminescence for patterned samples.

of crystals on different surfaces using this direct-write printer-type lithographic approach, we fabricated plastic substrate by paste plastic film on cardboard, and characterized the printed sample using SXRD. The SXRD data shown in Figure 2b clearly demonstrated the formation of crystals of **1**. However, the crystals of **1** on plastic substrate have smaller sizes, as compared to crystals on paper. As confirmed by SEM, crystals in plastic substrate with average edge were 300 ± 30 nm and 1.2 ± 0.5 μm, respectively (Figure 3d). This can be explained by considering the contact angles between the precursor solution and the surface. In hydrophobic surfaces, the contact angles were high and the affinity of the solution on the surface was low, so that printed droplets do not tend to spread completely once they are placed on the surface, promoting the formation of single crystals in reduced size. To evaluate the hydrophilicity of two substrates, contact angles were measured through the addition of a droplet of precursor solution on the substrate surface (Supporting Information Figure S5). The contact angles are 46.5° for paper substrate and 63° for plastic substrate, respectively. It is obvious that the hydrophilicity of paper substrate is higher than that of plastic substrate. This fact also demonstrates our deduction in some extent. The per-cycle printing can be finished within 10 min, including the evaporation process. This deposition speed reveals the high-throughput capability of the proposed technology.[29]

This fabrication methodology can also be used to precisely control the location at which a single LCCs crystal is grown. As shown in Figure 4a, China's treasure-panda was printed on paper substrate with high resolution after one printing−evaporation cycle (1cy) by using LCCs (**1**-Eu and **1**-Tb) inks (Supporting Information Figure S6). This printer technology can also realize the depositing of different LCCs in separated nozzles simultaneously. These characteristics have paved the way to design innovative platforms for creating barcodes. For a broad range of potential applications, we introduce **1**-Eu, **1**-Gd, and **1**-Tb, utilized as red, blue, and green emission sources, into separated ink cartridges, respectively, to construct a 2D barcode array system. As shown in Figure 4b, by varying the width, height, emission intensity, as well as the sequence of different lines, we can store a countless amount of cargo information. All of this information can only be detected under certain excitation (UV light), which may have potential application in the field of anticounterfeiting printing. Printing capacity has also been investigated by deposition of patterns in varied dimension; all samples from 1 mm to 10 cm exhibit high resolution. These results reveal that this technology is flexible and can be used widely (Supporting Information Figure S7).

Considering the well control of size and spatial location of LCC crystals, we try to introduce this technology for the development of luminescent device. As a proof-of-concept, we investigate the luminescent emission for **1**-Tb printed stamp in different cycles. With excitation at 295 nm, all of the emission spectra show green-luminescence with typical emission bands at 491, 544, 585, 622, and 648 nm, assigned to the $^5D_4 \rightarrow {}^7F_J$ (J = 6−2) transitions. As the number of printer cycles increases, the emission intensity grows gradually. As shown in Figure 5, the fluorescence intensity versus cycles plots can be curve-fitted into a linear relationship, which clearly reveals that the emission intensity can be digitally controlled by regulating print cycles. As compared to other depositing methods, such as spin-coating, layer by layer, and the vapor deposition method, such a printer technology exhibits overwhelming superiority in control of layer thickness and emission intensity.

Full-color luminescent materials, especially those with white color emission, have recently merited considerable attention because of their wide applications. It is well-known that the realization of full-color emission requires the generation and intensity control of the three fundamental red, green, and blue (RGB) light colors in bulk materials. Here, we apply this printer-type lithography technology in printing mixed-lanthanide luminescent emission, by varying the stoichiometric ratio of the gadolinium (blue emission), terbium (green emission), and europium (red emission) contents in the same ink cartridges. Various colors covering the whole visible range can be finely tuned. As shown in Figure 6, the emission spectra involve all of the emission peaks of the Tb^{3+}, Eu^{3+} ions and ligands to provide mixed peak contributions. It can be seen that the emission spectra of samples consist of a broad band and some weak lines. The former, centered at 410 nm, is due to the $\pi \rightarrow \pi^*$ electron transition of organic bridging ligands, while the latter peaks at 491, 544, 585, 622, and 648 nm are assigned to the characteristic $^5D_4 \rightarrow {}^7F_J$ (J = 6−2) transitions of Tb^{3+}. Emissions at 579, 592, 614, 651, and 694 nm are assigned to the characteristic $^5D_0$ excited state to the low-lying ^7F_J (J = 0, 1, 2, 3, and 4) levels of the Eu^{3+} ion. Here, because of the lowest excited states of the Gd^{3+}, its characteristic 4f−4f transition at 311 nm is not visible, and the broad blue-emission can be assigned to the luminescence of the ligand. All of the peaks have similar emission wavelengths, but various relative intensities depend on the ratios of the Tb^{3+}, Eu^{3+}, and Gd^{3+} ions in ink cartridges, resulting in a fluent change of their visible luminescent emission colors between green, blue, and red. Because white emission should ideally be composed of three red, green, and blue (RGB) primary colors and cover the whole visible range from 400 to 700 nm, we realized white-light emission with CIE (Commission International de L'Eclairage) chromaticity coordinates of (0.34, 0.35) by precise control of the Gd/Eu/Tb proportion, which is very close to that for pure white light (0.33, 0.33) according to the 1931 CIE coordinate diagram. Besides, multiple colors including pink, yellow green, and orange were achieved by varying the intensity ratio of RGB

emissions (Table 1 and Figure 7). Our results suggest that the construction of full-color luminescent materials based on printer-type lithography would be a promising strategy in the development of RGB-luminescent materials for use in the display field.

CONCLUSION

We reported a versatile printer-type lithography-based approach for growing LCC crystals on different supports, and realized the control growth of a submicrometer single crystal at a desired location on a surface. These results revealed a facile way in the command of special emission intensity, the control of particular emission in desired area, and the modulation of emission chromaticity. In addition, on the basis of our results, one may conceive to expand the scope of application for LCCs in sensors, magnetic, and electronic devices, etc.

ASSOCIATED CONTENT

Supporting Information

Instrument information data, and PXRD for synthesized sample. This material is available free of charge via the Internet at http://pubs.acs.org.

AUTHOR INFORMATION

Corresponding Author

*E-mail: zhj@fjirsm.ac.cn.

Notes

The authors declare no competing financial interest.

ACKNOWLEDGMENTS

We are thankful for support of this work by the National Basic Research Program of China (973 Programs 2011CB932504 and 2012CB821705) and NSFC (21221001, 91222105).

REFERENCES

(1) Cui, Y.; Yue, Y.; Qian, G.; Chen, B. Luminescent Functional Metal-Organic Frameworks. *Chem. Rev.* **2012**, *112*, 1126−1162.

(2) Moore, E.; Samuel, A.; Raymond, K. From Antenna to Assay: Lessons Learned in Lanthanide Luminescence. *Acc. Chem. Res.* **2009**, *42*, 542−552.

(3) Rocha, J.; Carlos, L.; Paz, F.; Ananias, D. Luminescent Multifunctional Lanthanides-Based Metal−Organic Frameworks. *Chem. Soc. Rev.* **2011**, *40*, 926−940.

(4) Feng, P. Photoluminescence of Open-Framework Phosphates and Germinates. *Chem. Commun.* **2001**, 1668−1669.

(5) Cui, Y.; Xu, H.; Yue, Y.; Guo, Z.; Yu, J.; Chen, Z.; Gao, J.; Yang, Y.; Qian, G.; Chen, B. A Luminescent Mixed-Lanthanide Metal−Organic Framework Thermometer. *J. Am. Chem. Soc.* **2012**, *134*, 3979−3982.

(6) Liu, Y.; Pan, M.; Yang, Q.; Fu, L.; Li, K.; Wei, S.; Su, C. Dual-Emission from a Single-Phase Eu−Ag Metal−Organic Framework: An Alternative Way to Get White-Light Phosphor. *Chem. Mater.* **2012**, *24*, 1954−1960.

(7) Guo, H.; Zhu, Y.; Qiu, S.; Lercher, J.; Zhang, H. Coordination Modulation Induced Synthesis of Nanoscale $Eu_{1-x}Tb_x$-Metal-Organic Frameworks for Luminescent Thin Films. *Adv. Mater.* **2010**, *22*, 4190−4192.

(8) Han, S.; Wei, Y.; Valente, C.; Forgan, R.; Gassensmith, J.; Smaldone, R.; Nakanishi, H.; Coskun, A.; Stoddart, J.; Grzybowski, B. Imprinting Chemical and Responsive Micropatterns into Metal−Organic Frameworks. *Angew. Chem., Int. Ed.* **2011**, *50*, 276−279.

(9) Majano, G.; Ramírez, J. Scalable Room-Temperature Conversion of Copper(II) Hydroxide into HKUST-1 ($Cu_3(btc)_2$). *Adv. Mater.* **2013**, *25*, 1052−1057.

(10) Witters, D.; Vergauwe, N.; Ameloot, R.; Vermeir, S.; Vos, D.; Puers, R.; Sels, B.; Lammertyn, J. Digital Microfluidic High-Throughput Printing of Single Metal-Organic Framework Crystals. *Adv. Mater.* **2012**, *24*, 1316−1320.

(11) Zhuang, J.; Ceglarek, D.; Pethuraj, S.; Terfort, A. Rapid Room-Temperature Synthesis of Metal−Organic Framework HKUST-1 Crystals in Bulk and as Oriented and Patterned Thin Film. *Adv. Funct. Mater.* **2011**, *21*, 1442−1447.

(12) Ameloot, R.; Roeffaers, M. B.; Cremer, G.; Vermoortele, F.; Hofkens, J.; Sels, B.; E, D. Metal−Organic Framework Single Crystals as Photoactive Matrices for the Generation of Metallic Microstructures. *Adv. Mater.* **2011**, *23*, 1788−1791.

(13) Sirringhaus, H.; Kawase, T.; Friend, R.; Shimoda, T.; Inbasekaran, M.; Wu, W.; Woo, E. High-Resolution Inkjet Printing of All-Polymer Transistor Circuits. *Science* **2000**, *290*, 2123−2126.

(14) Zhuang, J.; Friedel, J.; Terfort, A. The Oriented and Patterned Growth of Fluorescent Metal−Organic Frameworks onto Functionalized Surfaces. *Beilstein J. Nanotechnol.* **2012**, *3*, 570−578.

(15) Falcaro, P.; Buso, D.; Hill, A.; Doherty, C. Patterning Techniques for Metal Organic Frameworks. *Adv. Mater.* **2012**, *24*, 3153−3168.

(16) You, Y.; Yang, H.; Chung, J.; Kim, J.; Jung, Y.; Park, S. Micromolding of a Highly Fluorescent Reticular Coordination Polymer: Solvent-Mediated Reconfigurable Polymerization in a Soft Lithographic Mold. *Angew. Chem., Int. Ed.* **2010**, *49*, 3757−3761.

(17) Lu, G.; Farha, O.; Zhang, W.; Huo, F.; Hupp, J. Engineering ZIF-8 Thin Films for Hybrid MOF-Based Devices. *Adv. Mater.* **2012**, *24*, 3970−3974.

(18) Dimitrakakis, C.; Marmiroli, B.; Amenitsch, H.; Malfatti, L.; Innocenzi, P.; Grenci, G.; Vaccari, L.; Hill, A.; Ladewig, B.; Hill, M.; Falcaro, P. Top-down Patterning of Zeolitic Imidazolate Framework Composite Thin Films by Deep X-ray Lithography. *Chem. Commun.* **2012**, *48*, 7483−7485.

(19) Tsotsalas, M.; Umemura, A.; Kim, F.; Sakata, Y.; Reboul, J.; Kitagawa, S.; Furukawa, S. Crystal Morphology-Directed Framework Orientation in Porous Coordination Polymer Films and Freestanding Membranes via Langmuir−Blodgettry. *J. Mater. Chem.* **2012**, *22*, 10159−10165.

(20) Falcaro, P.; Lapierre, F.; Marmiroli, B.; Styles, M.; Zhu, Y.; Takahashi, M.; Hill, A.; Doherty, C. Positioning an Individual Metal−Organic Framework Particle Using a Magnetic Field. *J. Mater. Chem. C* **2013**, *1*, 42−45.

(21) Ricco, R.; Malfatti, L.; Takahashi, M.; Hill, A.; Falcaro, P. Applications of Magnetic Metal−Organic Framework Composites. *J. Mater. Chem. A* **2013**, *1*, 13033−13045.

(22) Zhang, H.; Shan, X.; Ma, Z.; Zhou, L.; Zhang, M.; Lin, P.; Hu, S.; Ma, E.; Li, R.; Du, S. A Highly Luminescent Chameleon: Fine-Tuned Emission Trajectory and Controllable Energy Transfer. *J. Mater. Chem. C* **2014**, *2*, 1367−1371.

(23) Li, W.; Gao, Y.; Liu, T.-F.; Han, L.-W.; Lin, Z.-J.; Cao, R. In Situ Growth of Metal−Organic Framework Thin Films with Gas Sensing and Molecule Storage Properties. *Langmuir* **2013**, *29*, 8657−8664.

(24) Park, Y.-S.; Lee, S.; Kim, K.-H.; Kim, S.-Y.; Lee, J.-H.; Kim, J.-J. Exciplex-Forming Co-host for Organic Light-Emitting Diodes with Ultimate Efficiency. *Adv. Funct. Mater.* **2013**, *23*, 4914−4920.

(25) Chen, X.-L.; Yu, R.; Zhang, Q.-K.; Zhou, L.-J.; Wu, X.-Y.; Zhang, Q.; Lu, C.-Z. Rational Design of Strongly Blue-Emitting Cuprous Complexes with Thermally Activated Delayed Fluorescence and Application in Solution-Processed OLEDs. *Chem. Mater.* **2013**, *25*, 3910−3920.

(26) Gans, B.; Duineveld, P.; Schubert, U. Inkjet Printing of Polymers: State of the Art and Future Developments. *Adv. Mater.* **2004**, *16*, 203−213.

(27) Sirringhaus, H.; Kawase, T.; Friend, R.; Shimoda, T.; Inbasekaran, M.; Wu, W.; Woo, E. High-Resolution Inkjet Printing of All-Polymer Transistor Circuits. *Science* **2000**, *290*, 2123−2126.

(28) Wu, Y.; Li, F.; Zhu, W.; Cui, J.; Tao, C.; Lin, C.; Hannam, P. M.; Li, G. Metal−Organic Frameworks with a Three-Dimensional Ordered

Macroporous Structure: Dynamic Photonic Materials. *Angew. Chem., Int. Ed.* **2011**, *50*, 12518−12522.
(29) Carbonell, C.; Imaz, I.; Maspoch, D. Single-Crystal Metal−Organic Framework Arrays. *J. Am. Chem. Soc.* **2011**, *133*, 2144−2147.
(30) Zhuang, J.; Ar, D.; Yu, X.-J.; Liu, J.; Terfort, A. Patterned Deposition of Metal-Organic Frameworks onto Plastic, Paper, and Textile Substrates by Inkjet Printing of a Precursor Solution. *Adv. Mater.* **2013**, *25*, 4631−4635.
(31) Chui, S.; Lo, S.; Charmant, J.; Orpen, A.; Williams, I. A Chemically Functionalizable Nanoporous Material $[Cu_3(TMA)_2(H_2O)_3]_n$. *Science* **1999**, *283*, 1148−1150.
(32) Zhang, H.; Shan, X.; Zhou, L.; Lin, P.; Li, R.; Ma, E.; Guo, X.; Du, S. Full-colour Fluorescent Materials Based on Mixed-lanthanide-(III) Metal−Organic Complexes With High-Efficiency White Light Emission. *J. Mater. Chem. C* **2013**, *1*, 888−891.
(33) Mooibroek, T.; Gamez, P.; Pevec, A.; Kasunič, M.; Kozlevcar, B.; Fu, W.-T.; Reedijk, J. Efficient, Stable, Tunable, and Easy to Synthesize, Handle and Recycle Luminescent Materials: $[H_2NMe_2]_3[Ln(III)(2,6\text{-dipicolinolate})_3]$ (Ln = Eu, Tb, or its solid solutions). *Dalton Trans.* **2010**, *39*, 6483−6487.